RSC Advances

PAPER

View Article Online
View Journal | View Issue

Cite this: *RSC Adv.*, 2022, **12**, 34185

Highly sensitive work function type room temperature gas sensor based on Ti doped hBN monolayer for sensing CO_2, CO, H_2S, HF and NO. A DFT study

Basheer Ahmed Kalwar, *[ab] Wang Fangzong, *[a] Amir Mahmood Soomro,[c] Muhammad Rafique Naich,[de] Muhammad Hammad Saeed [a] and Irfan Ahmed[b]

The adsorptions of toxic gas molecules (CO_2, CO, H_2S, HF and NO) on pristine and Ti atom doped hexagonal boron nitride (hBN) monolayer are investigated by density functional theory. Weak physisorption of gas molecules on pristine hBN results in micro seconds recovery time, limiting the gas sensing ability of pristine hBN. However Ti atom doping significantly enhances the adsorption ability. Ti atom best fits to be doped at B vacancy in hBN with lowest formation energy (−3.241 eV). Structural analysis reveals that structures of gas molecules change after being chemisorbed to Ti doped hBN monolayer. Partial density of states analysis illustrates strong hybridization among Ti-3d, gas-2p and BN-2p orbitals, moreover Bader charge transfer indicates that gas molecules act as charge acceptors. Ti doped hBN monolayer undergoes transition from semiconductor to narrow band semiconductor with adsorption of CO_2, H_2S and NO, while with CO and HF adsorption it transforms into metal. The change of conductance of Ti doped hBN monolayer in response to adsorption of gas molecules reveals its high sensitivity, however it is not selective to HF and NO gases. The recovery times of gas molecules desorption from monolayer are too long at ambient condition however it can significantly be shortened by annealing at elevated temperature with UV exposure. Since recovery time for NO removal from monolayer is still very long at 500 K with UV exposure, Ti doped hBN monolayer is more suitable as a scavenger of NO gas rather than as a gas sensor. It is thus predicted that Ti doped hBN monolayer can be a work-function type CO_2, CO, H_2S and HF sensor and NO gas scavenger.

Received 7th October 2022
Accepted 14th November 2022

DOI: 10.1039/d2ra06307g

rsc.li/rsc-advances

1. Introduction

Over the past few years, fossil fuel combustion, industrial processing and fast urbanization have caused the rapid and excessive emission of toxic and hazardous gases which threaten the human health and sustainability.[1,2] Hydrogen sulfide (H_2S) is a corrosive, flammable and no-color gas. It smells bad just like rotten eggs which can poison the nervous system of human body readily. Personnel of chemical safety and solid waste management use to set minimum limit of alarm detectors at 5–10 ppm of H_2S exposure.[3] Carbon monoxide (CO) is inodorous, un-irritant, colorless and non-annoying gas which means it is very difficult for anyone to sense. CO can easily cause hindered oxygen delivery and cellular oxygen uptake.[4] Carbon dioxide (CO_2) is the notorious gas which directly and indirectly damages the planet and increases global warming.[5] Hydrogen fluoride (HF) is widely used for cleaning and etching of industrial products. Due to its strong corrosive properties, a water diluted form of HF (*i.e.* hydrofluoric acid) is commercially available as anti-rusting and stain removing product. Gumi-4 industrial complex mishap reported in five fatalities and 18 severe injuries as result of HF leakage during its transfer between tanks in 2012.[6] Nitrogen monoxide (NO) is another toxic gas which can cause ozone damage, acidic rain and greenhouse effect.[7] Keeping the above mentioned facts and hazards in mind it is dire need to detect, monitor and remove toxic gases for safe and cleaner environment. In this regard, robust gas sensor that has selective, sensitive, rapid and reliable response in harsh environment is paramount.

[a]*College of Electrical Engineering and New Energy, China Three Gorges University (CTGU), Yichang 443002, China. E-mail: basheerahmed@ctgu.edu.cn; fzwang@ctgu.edu.cn*

[b]*Department of Electrical Engineering, Mehran University of Engineering and Technology, SZAB Campus, Khairpur Mirs 66020, Pakistan. E-mail: basheerahmed@muetkhp.edu.pk*

[c]*Department of Electrical Engineering, Mehran University of Engineering and Technology, Jamshoro 76062, Pakistan*

[d]*Department of Electronic Engineering, Mehran University of Engineering and Technology, SZAB Campus, Khairpur Mirs 66020, Pakistan*

[e]*School of Energy Science and Engineering, Harbin Institute of Technology, 92 West Dazhi Street, Harbin 150001, China*

Two dimensional (2D) materials *e.g.* graphene,[8] black phosphorene,[9] germanene and silicene,[10] aluminum nitride (AlN) and indium nitride (InN),[11] transition metal dichalcogenide (TMD)[12,13] and hexagonal boron nitride (hBN) monolayer[14] are now regarded as gas sensing materials due to their high surface to volume ratio, structural diversities and tunable opto-electronic properties. However, these materials are still practically immature to totally rely on due to certain complications and limitations. No dangling groups and zero band gap of intrinsic graphene hinder its practical applications of gas sensing.[15] Poor selectivity and sensitivity in harsh environment *i.e.* high temperatures is the bottleneck for practical applications of gas sensing of most 2D materials.[16] Therefore it is crucial to hunt for a material which should have fast response, good sensitivity and selectivity, total recovery and reliable operation at high temperatures. hBN commonly known as "white graphene" is one of the leading 2D material with distinct properties like higher thermal conductivity, high temperature structural stability and wide band gap making it robust gas sensing material used in harsh environments.[17] In a recent study, hBN sheet is seemed to be a good biosensor. A α-glucose molecule physisorbed on hBN sheet with −0.71 to −0.91 eV adsorption energy. The final structure remained highly stable and the good thing was that the electronic property of physisorbed system has shown semiconducting nature.[18] However, findings extracted from previous literature manifest that intrinsic hBN based gas sensors have no satisfactory results *i.e.* instantaneous recovery, slow response and poor selectivity.[19–21] The reason behind is the weak interactions of hBN monolayer with gas molecules due to inherent chemical inertness of hBN. Therefore researchers have countered this problem and enhanced the gas sensing by surface activation through,[22,23] foreign element doping[24–26] and defect engineering.[27,28] It has been proved that metal decoration on 2D materials can significantly enhance the gas adsorption affinity of 2D materials.[29,30] Ramirez-de-Arellano *et al.* have checked the CO interaction with hBN monolayer by six models; B-vacancy hBN, N-vacancy hBN, Ti doped in N-vacancy, Ti doped in B-vacancy, Pt doped in N-vacancy and Pt doped in B-vacancy. hBN monolayer with B and N vacancy could not hold CO molecule whereas, Ti and Pt doped at N-vacancy and B-vacancy held CO molecule by chemisorptions with 1.69 eV, 1.53 eV, 1.16 eV and 2.10 eV adsorption energies respectively.[31] In another study, the authors have doped Ti at Stone Wales defect (Ti_{SW}) site and at N-vacancy (Ti_{Nv}) site in hBN monolayer to adsorb N_2 gas for production of ammonia (NH_3). Reaction energy barrier for NH_3 production has greatly decreased as result of both Ti_{SW} and Ti_{Nv} doping structures. Further, Ti doping enhanced the catalytic activity by decreasing the band gap of hBN monolayer.[32] Recently in a DFT study, five types of gas molecules (H_2, N_2, CO, NO and CO_2) were adsorbed on twelve metals (Ag, Au, Co, Cr, Cu, Fe, Mn, Na Pd, Pt, Ti and V) doped hBN monolayer systems. Metal atoms doped at B-vacancy site bonded strongly to sheet than doped at N-vacancy site. Ti doped hBN system found to be the structurally strongest system with a 12.9 eV binding energy. NO and CO gases were captured most easily by Pt doped hBN system.[33] Anota E. C. activated the boron nitride nano-sheet by replacing basic hexagon of boron nitride nano-sheet with homo-nuclear atoms (boron) at its center. Concentration of higher negative charge appeared at triangular and pentagonal structures due to boron atoms population. Negative charge concentration attracted various molecules and enhanced the drug sensing affinity.[34]

It is well known that high quality 2D hBN have been successfully prepared by molecular beam epitaxy (MBE), chemical vapor deposition (CVD) and metal–organic chemical vapor deposition (MOCVD).[20,35] The electronic and magnetic properties of hBN can greatly be altered by transition metal atoms doping. Avoiding noble atoms, a commonly used 3d transition metal atoms doping can activate the surface in a cost effective and non-toxic way. Even though $(TiO_2)_{19}$ cluster is used as host material for trapping H_2, CO and CO_2 molecules, the Ti atom site was found to be most preferred adsorption site rather than O atom site. This shows that Ti atom among other inline elements has more trapping affinity.[36] It has been concluded from above literature that Ti decorated hBN monolayer has been found good catalyst and gas storage material.[37,38] However, no study has been reported using Ti doped hBN monolayer as gas sensing material for CO_2, CO, H_2S, HF and NO. Therefore, a detailed study containing structural and electronic properties of gas adsorbed systems is an urgent need.

In this work, at first we have investigated the gas sensing (adsorption) ability of pristine hBN for above toxic gases (CO_2, CO, H_2S, HF and NO). The adsorption ability is evaluated by adsorption energy, adsorption distance and recovery time whereas the sensitivity is evaluated by the variation in electronic properties and work function. Since the scope of this study is sensing the toxic gas molecules, therefore variation in band gap (electronic property) before and after gas adsorption is taken as key result. Therefore we have used HSE06 functional for electronic properties calculations to precisely calculate the band gap energy. The weak physisorption of gas molecules on pristine hBN led to desorption within microseconds. The change in electronic properties of pristine hBN in response to weak physisorption of gas molecules is not anticipated due to very short recovery time. Therefore, Ti atom was doped in three different defect sites in pristine hBN to find the most energetic system for activation of the surface for gas sensing. Ti doped at B vacancy site was found to be the most energetically stable system, hence selected as final gas sensing material (Ti doped hBN monolayer). To further verify the suitability of Ti doped hBN monolayer as gas sensor in high temperatures, thermodynamic stability of selected system was also evaluated by first principle molecular dynamics (FPMD) at 300, 500, 1000 and 1200 K for 3500 fs simulation time. FPMD analysis showed that there was no any significant distortion in structure at 1000 K. After all, we investigated the adsorption ability (gas sensing) of Ti doped hBN monolayer for CO, CO_2, H_2S, HF and NO gas molecules by first principle calculations. Moreover, the structural stability of our systems can be corroborated by findings of a study, where authors have confirmed that neither vacancy defect nor elemental doping leads to structural instability. However point defects shorten the band gap of the boron nitride.[39] The gas sensing ability of Ti doped hBN monolayer is verified by structural, electronic, sensitivity and application

feasibility analyses. The structural properties are supported with adsorption energy, adsorption distance whereas electronic properties are carried with partial density of states (PDOS) and Bader charge transfer.[40] The sensitivity and selectivity analysis is evaluated by electronic band structures and work function. Application feasibility of Ti doped hBN monolayer is supported with FPMD simulations at room temperature and recovery times at room temperature, 400 and 500 K with visible and UV exposures. We found that pristine hBN cannot sense the gas molecules, however doping of Ti atom in hBN could greatly enhance the sensing ability of hBN to all five gas molecules. Ti doped hBN monolayer aced as sharp responsive, highly sensitive and selective with less recovery time toxic gas sensor.

2. Computational details

All the calculations were carried out with spin polarized DFT calculations using Vienna *ab initio* simulation package (VASP).[41] Generalized gradient approximation (GGA) with Perdew–Burke–Ernzerhof (PBE) functional was used to describe the exchange correlation potential.[42] A plane wave basis set was employed within the framework of projector augmented wave (PAW) method.[43] The energy cut-off was taken to be 460 eV for wave function expansion. The convergence criteria for energy and structural relaxation on each atom were set to 10^{-6} eV and 0.02 eV $Å^{-1}$. In order to get satisfactory convergence of all structures, a 9 × 9 × 1 Monkhorst–Pack *k*-point grid was employed to sample the Brillouin zone (BZ).[44] To consider weak van der Waals (vdW) interactions, Grimme's DFT-D2 approach was applied.[45] Chances of interaction of periodic images were discarded by inserting 18 Å space in *z*-direction. Bader charge analysis was employed to calculate the charge distribution and charge transfer between hBN monolayer, doped Ti atom and toxic gas molecule.[46] All the structures and charge density difference (CDD) diagrams were visualized with VESTA.[47]

3. Results and discussion

3.1. Structures of pristine hBN, isolated gas molecules and adsorption of gas molecules on pristine hBN monolayer

3.1.1. Structural analysis of pristine hBN monolayer. A 4 × 3 × 1 supercell of hBN monolayer was modeled as basic structure which contains 12 B and 12 N atoms as shown in Fig. 2a. After structural relaxation, the resultant structure of hBN has planar geometry like graphene and bond length of B–N is 1.418 Å. It is also found that hBN monolayer has semiconducting characteristic with direct band gap of 5.17 eV, which is closely comparable to previous work.[32,48] It indicates that calculation method is valid for this system to further carryout other calculations.

3.1.2. Structures of isolated gas molecules. Before verifying the gas sensing performance of pristine hBN and Ti doped hBN monolayer, the structures of isolated gas molecules are optimized as shown in Fig. 1. The obtained bond lengths of CO_2 (O–C and C–O), CO (C–O), H_2S (H–S and S–H), HF (H–F), NO (N–O) gas molecules are 1.19, 1.43, 1.38, 0.91 and 1.16 Å respectively. The bond angles, O–C–O of CO_2 and H–F–H of H_2S gas molecules are 180° and 92.1° respectively. These values of structural parameters of gas molecules in our work are consistent with previous reports.[49–51]

3.1.3. CO_2, CO, H_2S, HF and NO adsorption on pristine hBN monolayer. To explore the gas sensing property of hBN monolayer, we studied the adsorption of CO_2, CO, H_2S, HF and NO gas molecules on pristine hBN monolayer. Various adsorption sites (B top, N top, B–N bridge) are selected as input geometries. The gas sensing performance of any gas sensing material can be assessed at first instant by adsorption energy (E_{ads}) *i.e.* interaction strength of gas sensing material with gas molecules, charge transfer (Δq), variation of electronic property and recovery time (τ). The expression for calculating the adsorption energy (E_{ads}) is as following.

$$E_{ads} = E_{gas+hBN} - E_{hBN} - E_{gas} \quad (1)$$

where $E_{gas+hBN}$, E_{hBN} and E_{gas} are representing the total energies of optimized systems of gas molecule adsorbed on pristine hBN monolayer, pristine hBN monolayer without gas molecule and gas molecule only respectively.

The recovery time is meant the time required for any gas molecules to fully dislodge from adsorbent, which is calculated by expression (2). The values of adsorption energies of gas molecules adsorbed on pristine hBN monolayer are 0.16, 0.21, 0.34, 0.27 and 0.19 eV for CO_2, CO, H_2S, HF and NO respectively. These small values of adsorption energies prove that the gas

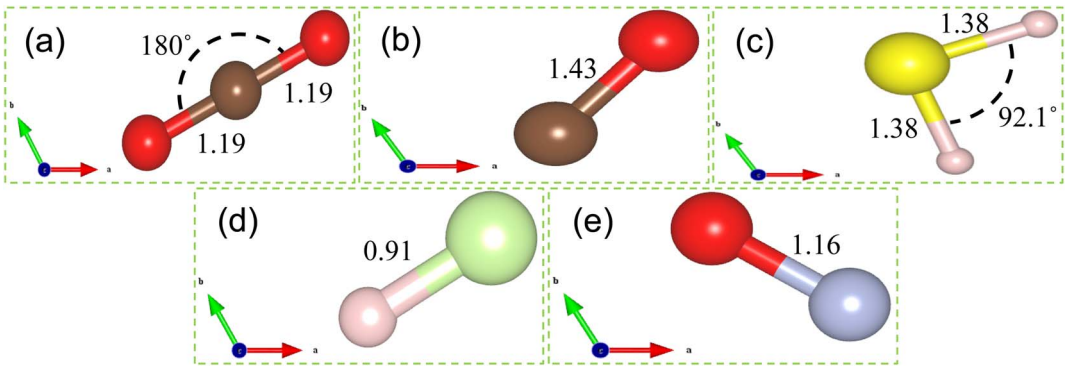

Fig. 1 Isolated molecules of (a) CO_2, (b) CO, (c) H_2S, (d) HF and (e) NO. Red, brown, yellow, blush and light green balls denote O, C, S, H and F atoms respectively.

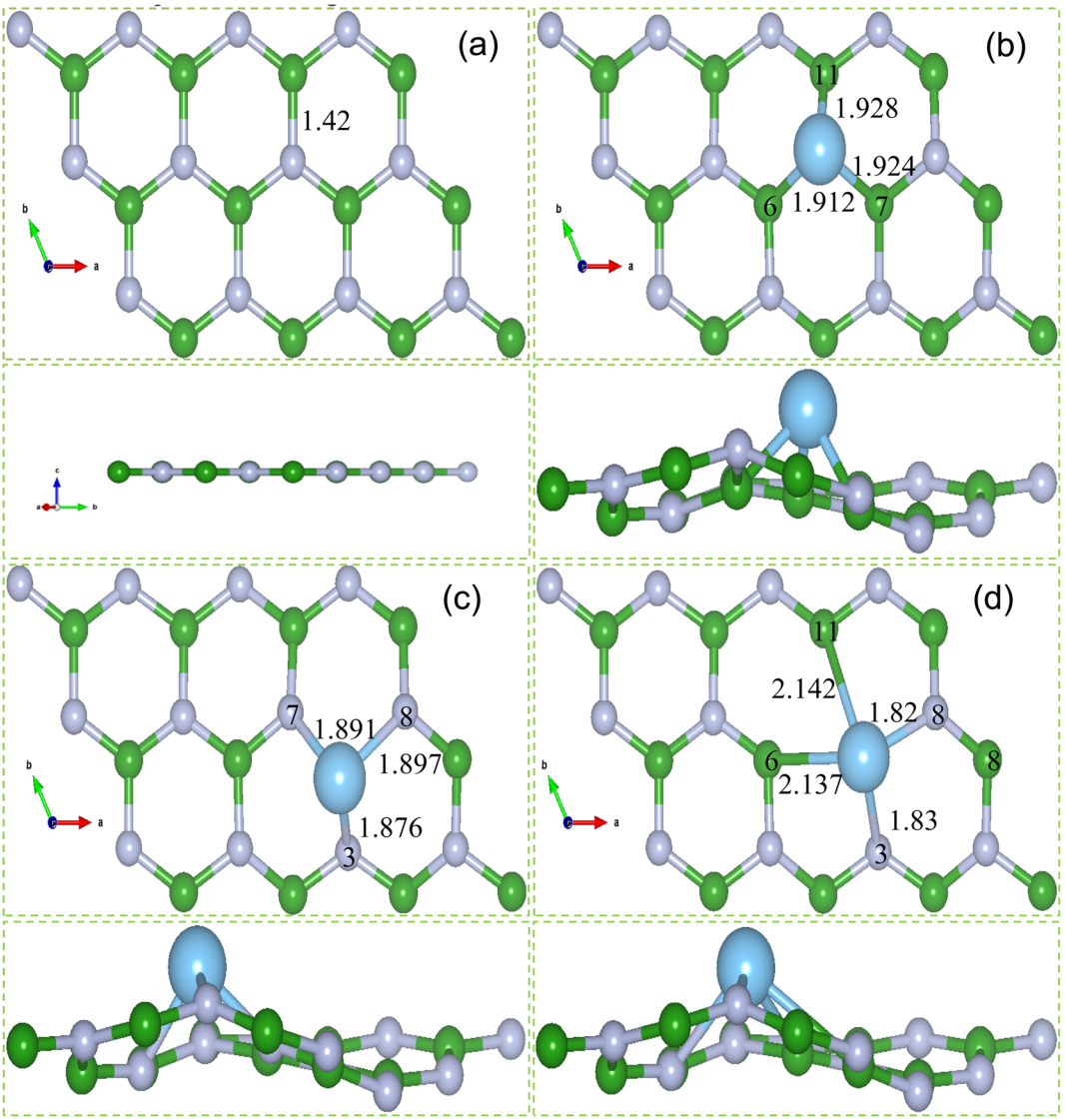

Fig. 2 Top and side views of (a) pristine hBN monolayer and optimized structures of (b) Ti_V_N-hBN, (c) Ti_V_B-hBN and (d) Ti_V_{SW}-hBN. Green, light gray and light blue balls denote B, N and Ti atoms respectively.

molecules are physisorbed. Further, Bader charge analysis shows that CO_2, CO and NO donate very small charge of 0.011, 0.014 and 0.013*e* to hBN monolayer, while H_2S and HF withdraw 0.071 and 0.067*e* from hBN monolayer respectively. From transition state theory,[52] the recovery time (τ) of a gas sensor is the time required for analytes to be desorbed from the surface, is

$$\tau = \upsilon_o^{-1}\, \mathrm{e}^{\left(-\frac{E_{bp}}{K_B T}\right)} \quad (2)$$

Here, T is the test temperature in K, K_B is Boltzmann constant (8.62×10^{-5} eV K^{-1}) and E_{bp} is potential barrier for desorption of gas molecules. Since adsorption and desorption of gas molecules are opposite processes to each other, thus the value of adsorption energy E_{ads} can be substituted in E_{bp}. υ_o indicates the attempt frequency, which is 10^{12} Hz at room temperature.[53]

The values of recovery time at room temperature with visible light exposure (10^{12} Hz attempt frequency) are 4.82×10^{-10}, 3.361×10^{-9}, 5.088×10^{-7}, 3.420×10^{-8} and 1.551×10^{-9} seconds for CO_2, CO, H_2S, HF and NO gas molecules respectively. Such microsecond recovery time is too small (instantaneous desorption) to make electronic properties of hBN monolayer alter. Therefore pristine hBN monolayer cannot be supposed to be a practical gas sensor of above gases at room temperature. Further, the values of adsorption energy (E_{ads}), adsorption distance (D), charge transfer (Δq) and recovery time (τ) of most stable structures of gas molecules adsorbed on pristine hBN monolayer are tabulated in Table 1.

3.2. Ti doping at N vacancy, B vacancy and Stone Wales defect in hBN monolayer

As discussed in previous section, low adsorption energy, small charge transfer and microsecond recovery time of gas molecules

Table 1 Results of most stable structures of CO_2, CO, H_2S, HF and NO gas molecules adsorbed on pristine hBN and Ti doped hBN monolayer. E_{ads} (in eV) is adsorption energy of gas molecules adsorbed on pristine and Ti doped hBN monolayer. D (in Å) is the adsorption distance, the shortest distance between atom of gas molecule and monolayer. Δq (in e) are the number of electrons transfer between gas molecules, pristine hBN and Ti doped hBN monolayer. Negative sign indicates charge transferred to gas molecules whereas positive sign indicates charge transferred from gas molecules. E_g (in eV) is band gap. Φ (in eV) is the work function

	Pristine hBN			Ti doped hBN monolayer				
System	E_{ads} (eV)	D (Å)	Δq (e)	E_{ads} (eV)	D (Å)	Δq (e)	E_g (eV)	Φ (eV)
Ti-hBN	—	—	—	—	—	—	2.61	5.31
CO_2	0.16	2.91	+0.011	−1.32	2.09	−0.18	0.98	4.82
CO	0.21	2.86	+0.014	−1.66	2.01	−0.21	0	4.70
H_2S	0.34	2.24	−0.071	−1.20	1.88	−0.16	0.33	4.88
HF	0.27	2.51	+0.067	−0.81	2.16	−0.10	0	4.91
NO	0.19	2.84	−0.013	−1.82	2.10	−0.28	0.11	4.48

adsorbed on pristine hBN monolayer conclude that pristine hBN has negligible sensitivity of above gas molecules. It is also well known that appropriate surface modification by 3d transition metal atom decoration greatly enhance the gas adsorption ability of 2D materials.[54] Therefore we have decorated the hBN monolayer with titanium (Ti) atom. Since Ti is a 3d transition metal and there exist a problem of metal aggregation due to strong d–d interaction of transition metal (TM) atoms when 2D materials are decorated with them. To solve this problem, it is proposed to anchor the TM atom through defect in host material.[55,56] Therefore we have doped the Ti atom by creating defects in hBN monolayer as Ti doped at N vacancy (Ti_V_N-hBN), at B vacancy (Ti_V_B-hBN) and at Stone Wales defect (Ti_V_{SW}-hBN) systems. For this purpose we ejected an adjacent N atom, B atom and both N and B step by step from 4 × 3 × 1 supercell of hBN monolayer to form N vacancy (V_N-hBN), B vacancy (V_B-hBN) and Stone Wales defect (V_{SW}-hBN). After creating vacancy in hBN monolayer, we embedded Ti atom on the vacancy site and allowed the structures to relax. The relaxed structures no longer sustained the same bond lengths as shown in Fig. 2b–d. The Ti atom forms three bonds in V_N-hBN and V_B-hBN structures with adjacent B and N atoms and four bonds in V_{SW}-hBN with adjacent B and N atoms. As Ti atom protrudes upwards higher than the plane of hBN monolayer, the bonded N and B atoms also stretch upwards, making the overall formation a bit more stable like buckled structure.

To determine the structural stability of doping structure, we calculated the formation energies (E_f) by using following expression.

$$E_f = E_{Ti\text{-}hBN} - \mu_{Ti} + m\mu_B + n\mu_N - E_{pristine\ hBN} \quad (3)$$

Here, $E_{Ti\text{-}hBN}$, $E_{pristine\ hBN}$ are total energies obtained from a supercell calculation with and without Ti doping hBN monolayer. μ_{Ti}, $n\mu_B$ and $n\mu_N$ are chemical potentials of Ti, B and N atoms respectively, whereas n is the number of atoms of B and N.

To evaluate the bonding strength of Ti atom with hBN monolayer, the binding energy (E_b) was calculated by employing following expression.

$$E_b = E_{Ti\text{-}hBN} - E_v - E_{Ti} \quad (4)$$

where $E_{Ti\text{-}hBN}$, E_v and E_{Ti} are representing the total energies of optimized systems of Ti doped hBN monolayer, defective hBN (nitrogen atom vacancy V_N, boron atom vacancy V_B, Stone Wales vacancy V_{SW}) and Ti atom respectively.

The binding energy and charge transfer between dopant atom and monolayer can be used to assess the structural stability of a 2D material. Binding energy (E_b), net Bader charge and bond lengths of pristine hBN, Ti_V_N-hBN, Ti_V_B-hBN and Ti_V_{SW}-hBN systems are listed in Table 2. The average bond lengths of B–N surrounding the dopant site in Ti_V_N-hBN, Ti_V_B-hBN and Ti_V_{SW}-hBN systems are 1.416, 1.411 and 1.395 Å respectively, which are smaller than 1.420 Å in pristine hBN. It shows that the doping of Ti atom causes the overall structures somehow corrugated. The bond lengths of three B atoms in Ti_V_N-hBN system are Ti–B_6 = 1.912, Ti–B_7 = 1.924 and Ti–B_{11} = 1.928 Å. Similarly, the bond lengths of three N atoms in Ti_V_B-hBN are Ti–N_3 = 1.876, Ti–N_7 = 1.891 and Ti–N_8 = 1.897 Å. These bond lengths of Ti–B and Ti–N are longer than bond length of B–N of pristine hBN before doping which shows the protrusion of the Ti atom. On other side, the bond lengths of B and N atoms in Ti_V_{SW}-hBN system are larger than B–N,

Table 2 The formation energy (E_f), binding energy (E_b), net Bader charge (e), bond length of Ti, B and N in V_N-hBN, V_B-hBN and V_{SW}-hBN

System	E_f (eV)	E_b (eV)	Net Bader charge (e)		Bond length (Å)	
Pristine hBN	—	—	N	−1.97	B–N	1.420
			B	+1.97		
Ti_V_N-hBN	−0.891	−5.45	Ti	−1.254	B–N	1.416
			B_6	+0.471	Ti–B_6	1.912
			B_7	+0.631	Ti–B_7	1.924
			B_{11}	+0.631	Ti–B_{11}	1.928
Ti_V_B-hBN	−3.241	−12.7	Ti	+1.157	B–N	1.411
			N_3	−1.40	Ti–N_3	1.891
			N_7	−1.39	Ti–N_7	1.876
			N_8	−1.33	Ti–N_8	1.897
Ti_V_{SW}-hBN	−1.765	−9.89	Ti	+1.505	B–N	1.395
			B_6	+0.766	Ti–B_6	2.137
			B_{11}	+0.644	Ti–B_{11}	2.142
			N_3	−2.102	Ti–N_3	1.830
			N_8	−2.087	Ti–N_8	1.820

however protrusion of Ti atom takes place comparatively shorter.

Bader charge analysis shows that net Bader charges on three B atoms bonded to Ti atom in Ti_V_N-hBN system decreases from +1.97*e* of pristine hBN to +0.471, +0.631 and +0.631*e*. The decrease in net Bader charges on B atoms after Ti atom is doped show that Ti has transferred 0.71*e* to B atoms, finally making Ti has +1.254*e* net Bader charge. In the case of Ti_V_B-hBN system, the three N atoms bonded to Ti atom have accumulated 0.81*e* charge after Ti doping. The net Bader charge on Ti atom appears as +1.157*e* which is lesser than net Bader charge on B atom in pristine hBN. For Ti_V_{SW}-hBN system, after Ti atom is doped, 0.46*e* charges have transferred from Ti atom to bonded B and N atoms, finally making Ti atom has +1.505*e* net Bader charge. The net Bader charges on B atoms bonded to Ti atom have decreased from +1.97 to +0.766 and +0.644*e*. While the two N atoms bonded to Ti atom have accumulated the charge and net Bader charges on N atoms have increased from −1.97 to −2.102 and −2.087*e*. It is worth noting here that due to more charge transfer from Ti atom to N atoms as compared to B atoms, the bond lengths of Ti–N are shorter than Ti–B.

As shown in the Table 2, the calculated formation energies of Ti_V_N-hBN, Ti_V_B-hBN and Ti_V_{SW}-hBN systems are 0.891, −3.241 and −1.765 eV respectively. This suggests that Ti atom can easily be doped at B atom site compared to N and BN site. This result is consistent with results of a study in which it is proved that doping at B vacancy is more energetically stronger than N vacancy and BN vacancy.[57,58] Further, the values of binding energies and charge transfer in Ti_V_N-hBN, Ti_V_B-hBN and Ti_V_{SW}-hBN systems are −5.45, −12.7 and −9.89 eV and 0.71, 0.81 and 0.46*e* respectively. Since Ti_V_B-hBN system has lowest formation and binding energies and there are a bit more charges transfer than the other two systems. It is therefore Ti_V_B-hBN system is selected as final structure and is considered in the subsequent calculations for the gas sensing. Lastly, Ti_V_B-hBN system is hereby referred as Ti doped hBN monolayer for rest of the work.

3.2.1. First principle molecular dynamics of Ti doped hBN monolayer. To verify the feasibility of Ti doped hBN monolayer (Ti_V_B-hBN) as gas sensing material for harsh environments, we investigated the thermodynamic stability. For this we have performed the first principle molecular dynamic (FPMD) simulations by using Nose–Hoover thermostat algorithm. The total energies of Ti doped hBN monolayer calculated at 300, 500, 1000 and 1200 K temperatures are shown in Fig. 3. The final structures after 4 ps simulation time are also displayed as insets. From Fig. 3 it is clear that total energy of Ti doped hBN monolayer during FPMD up to 1000 K keeps oscillations within a small range, indicating that the crystal structure of Ti doped hBN monolayer remains thermodynamically stable till 1000 K temperature. Further, at a temperature of 1200 K, the total energy of Ti doped hBN monolayer oscillates comparatively in

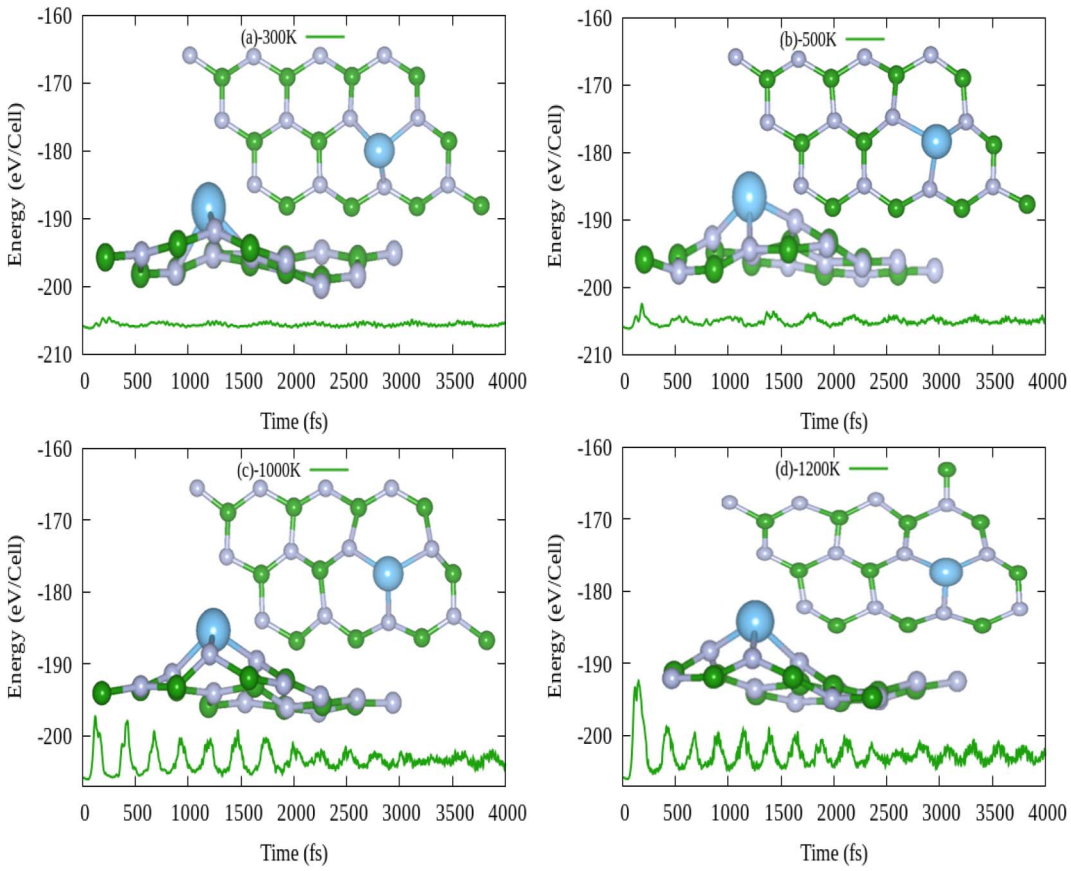

Fig. 3 The fluctuation of total energy of Ti doped hBN monolayer during FPMD simulations at (a) 300, (b) 500, (c) 1000, (d) 1200 K. The insets in (a–d) are the top and side views of final structures after 4 ps simulation time.

a wider range and the structure begins to distort when temperature rises above 1200 K. The final structure and total energy profiles under 1200 K indicate that Ti doped hBN monolayer can be used as gas sensor in elevated temperatures.

3.3. Adsorption of CO_2, CO, H_2S, HF and NO molecules on Ti doped hBN monolayer

The adsorption structures of different gas molecules adsorbed on Ti doped hBN monolayer are considered systematically. To get the most energetically stable structures, several possible adsorption configurations were analyzed and each was fully relaxed. The adsorption energy of gas molecules adsorbed on Ti doped hBN monolayer is calculated by following expression.

$$E_{ads} = E_{gas+Ti\text{-}hBN} - E_{Ti\text{-}hBN} - E_{gas} \quad (5)$$

where $E_{gas+Ti\text{-}hBN}$, $E_{Ti\text{-}hBN}$ and E_{gas} are representing the total energies of optimized systems of gas molecule adsorbed on Ti doped hBN monolayer, Ti doped hBN monolayer without gas molecule and gas molecule only respectively.

The most stable structures of gas molecules adsorbed on Ti doped hBN monolayer are portrayed in Fig. 4. The obtained adsorption energy (E_{ads}), adsorption distance (D) and charge transfer (Δq) between gas molecule and Ti doped hBN monolayer are listed in Table 1. The calculated adsorption energies of CO_2, CO, H_2S, HF and NO gas molecules adsorbed on Ti doped hBN monolayer are −1.32, −1.66, −1.20, −0.81 and −1.82 eV respectively. The negative values of adsorption energies indicate that adsorption of gas molecules on Ti doped hBN monolayer occur through exothermic reaction and energetically favorable.

3.3.1. Structural analysis of CO_2, CO, H_2S, HF and NO molecules on Ti doped hBN monolayer. The gas molecules were addressed on top of impurity site (Ti atom top). It was done due to protrusion of Ti atom above the hBN monolayer surface that can adsorb the gas molecules more easily. Furthermore, various adsorption configurations were considered to analyze the interaction between Ti doped hBN monolayer and gas molecules. C atom of CO_2 over Ti ($\underline{C}O_2$), any O atom of CO_2 over Ti ($C\underline{O}_2$), similarly for CO molecule ($\underline{C}O$) and ($C\underline{O}$), any H atom of H_2S molecule on Ti ($\underline{H}_2S$), S atom on Ti ($H_2\underline{S}$), H atom of HF on Ti ($\underline{H}F$), F on Ti ($H\underline{F}$) and N atom over Ti ($\underline{N}O$), O on Ti ($N\underline{O}$) were considered as input geometries. Similar strategy is made in ref. 59 and 60 to search the most stable structure with minimum energy. Among all input geometries, the most energetically stable structures of CO_2, CO, H_2S, HF and NO gas molecules adsorbed on Ti doped hBN monolayer are shown in Fig. 4. All the gas molecules are chemisorbed on Ti doped hBN monolayer, which is concluded by their adsorption energies (E_{ads}), charge transfer (Δq) values above 0.80 eV, 0.10e respectively and adsorption distance (D) generally around 2 Å. Further we found that the values of adsorption energy of CO_2, CO, H_2S, HF and NO on Ti doped hBN monolayer are negative, indicating that the adsorption of these gas molecules on Ti doped hBN monolayer is energetically favorable (see Table 1). In Fig. 4, it

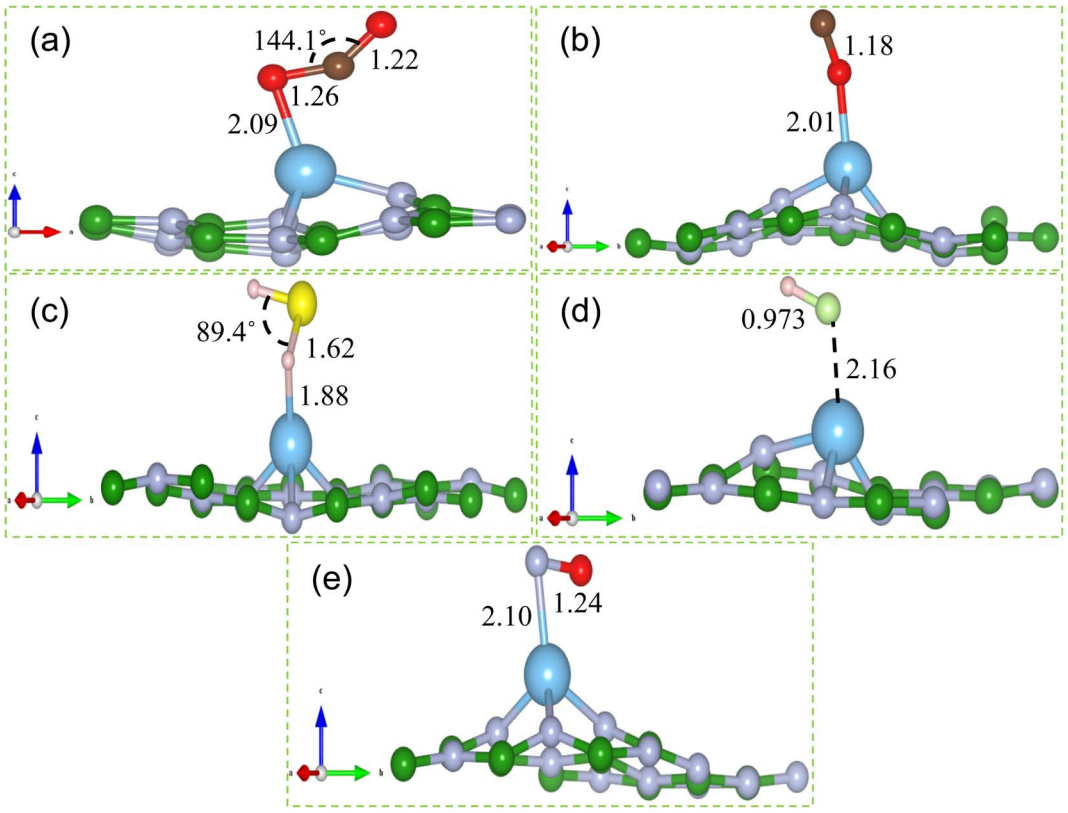

Fig. 4 Most stable structures of Ti doped hBN monolayer exposed to (a) CO_2, (b) CO, (c) H_2S, (d) HF and (e) NO molecule. Green, light gray, light blue, red, brown, yellow, blush and light green balls denote B, N, Ti, O, C, S, H and F atoms respectively.

can be clearly seen that the gas molecules adsorbed on Ti doped hBN monolayer locate mostly on protruded Ti atom. For CO_2 molecule, O atom is bonded to the Ti atom with O–Ti bond length of 2.09 Å, while the straight structure of CO_2 changed to angled one with O–C–O 144.1°. Similar deformation of CO_2 structure is noticed when adsorbed on TM functionalized 2D materials in previous reports.[33,51] The O–C and C–O bond lengths of CO_2 increase from 1.19 to 1.26 and 1.22 Å, indicating strong interaction between CO_2 molecule and Ti doped hBN monolayer. As for CO, the adsorption distance is measured to be 2.01 Å. The adsorbed CO molecule is nearly vertical to the plane of Ti doped hBN monolayer. The bond length of C–O decreases to 1.18 Å, shorter than that of isolated CO 1.43 Å. In regard to H_2S, the molecule gets adsorbed above the Ti atom with H atom inclined to Ti atom. The bond length of S–H elongated to 1.62 Å, longer than that of isolated H_2S 1.38 Å, while the bond angle decreases to 89.4°. HF molecule prefers to be adsorbed at a position horizontal to hBN plane with a small slope and the bond length of H–F stretches from 0.91 to 0.973 Å. The small bond length variation implies that there is comparatively weak interaction between HF and Ti doped hBN monolayer. For NO molecule, the gas molecule stays horizontal to Ti doped hBN

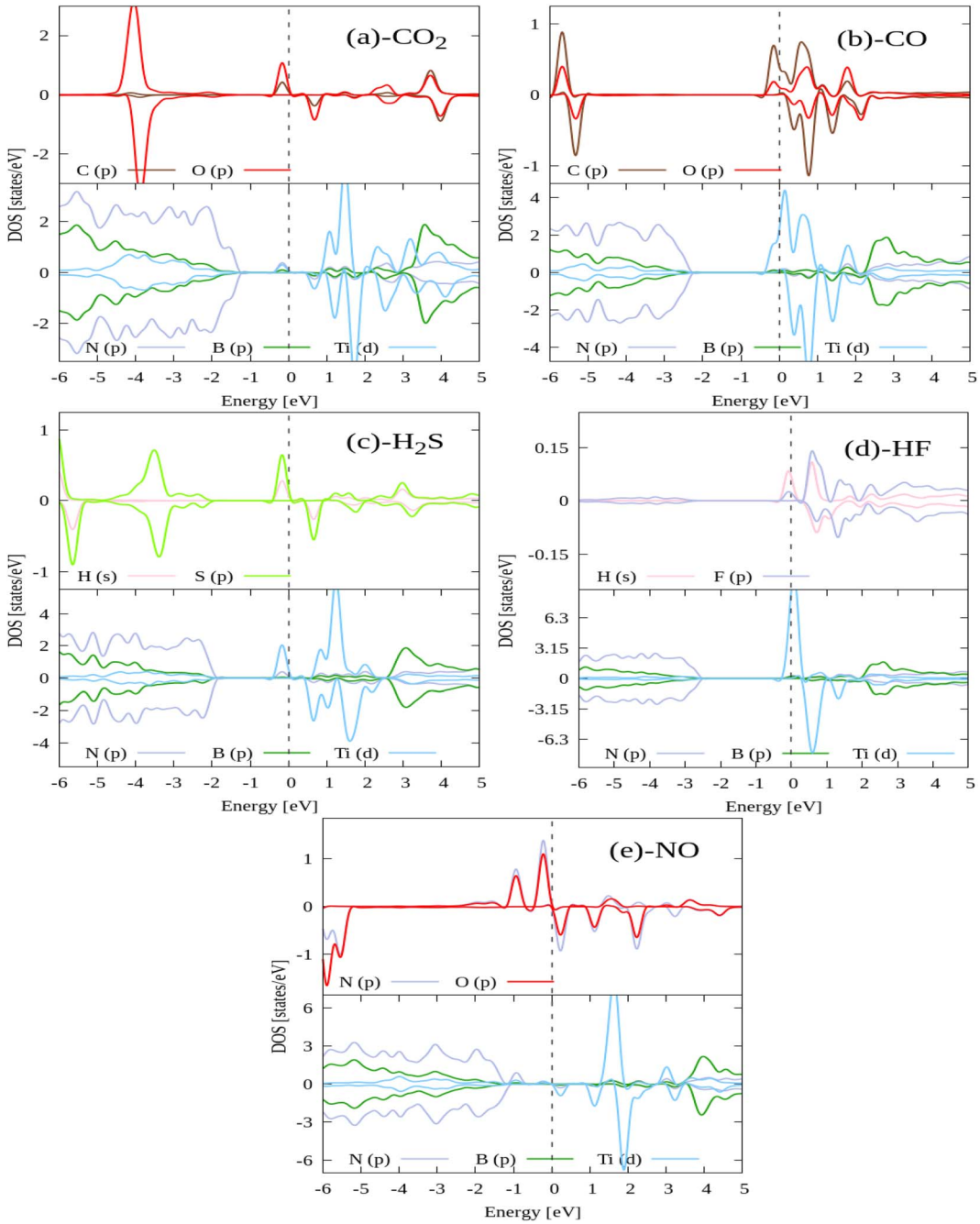

Fig. 5 Partial density of states (PDOS) of Ti doped monolayers exposed to (a) CO_2, (b) CO, (c) H_2S, (d) HF and (e) NO gas molecules. The Fermi energy is set at zero denoted by vertical black dashed line.

monolayer with O atom just 2.12 Å above the Ti atom. The bond length of N–O increases to 1.24 Å, longer than that of isolated NO 1.16 Å.

The atomic radii of B, N, Ti, C, O, H, S and F are 0.87, 0.56, 1.76, 0.67, 0.48, 0.53, 0.88 and 0.42 Å respectively.[61] According to Table 1, the adsorption distances between Ti and CO_2 (Ti–O), CO (Ti–O), H_2S (Ti–H), HF (Ti–F) and NO (Ti–N) are 2.09, 2.01, 1.88, 2.16 and 2.10 Å respectively, while the sums of corresponding atomic radii are 2.24, 2.24, 2.29, 2.18 and 2.32 Å respectively. It can be concluded that the calculated values of adsorption distance are less than the sums of corresponding atomic radii, suggestive of covalent bond between Ti and gas molecules. Hence, it is proved that all the gas molecules are chemisorbed to Ti doped hBN monolayer.

3.3.2. PDOS and charge transfer analysis of CO_2, CO, H_2S, HF and NO molecules on Ti doped hBN monolayer. To elucidate the mechanism of gas molecules adsorption on Ti doped hBN monolayer, the spin polarized PDOS is presented in Fig. 5. The Fig. 5a clearly shows that the C 2p and O 2p orbitals of CO_2 have multiple overlaps with Ti 3d at −4.0, −0.1, 1.5 in spin up and at −3.8, 0.5, 3.8 eV in spin down. The spin up and spin down states of CO_2 and Ti doped hBN monolayer are not symmetric, hence the spin splitting of DOS occurs and thus CO_2 adsorbed on Ti doped hBN monolayer exhibited magnetic nature. The obtained total magnetic moment of the system is 0.706 μ_B. For the CO molecule, as shown in Fig. 4b, the C 2p and O 2p orbitals of CO have certain hybridization peaks with Ti 3d at −5.8, −0.1, 1 eV in spin up and at −5.2, 1 eV in spin down. The spin up and spin down states are asymmetric and the obtained total magnetic moment of the system is 0.741 μ_B. In H_2S adsorbed system, the H 1s and S 2p orbitals of H_2S have two hybridization peaks with Ti 3d at −0.1 eV in spin up and at 0.5, 1.7 eV in spin down. The spin splitting of DOS of H_2S and Ti doped hBN monolayer occurred resulting in obtained total magnetic moment of 0.684 μ_B. As for the adsorption of HF molecule, the H 1s and F 2p orbitals of HF are localized and have hybridization peak at Fermi in spin up and at 0.5 eV in spin down. Fewer hybridization peaks of HF and Ti doped hBN monolayer indicate comparatively small charge transfer and adsorption energy. The spin up and spin down states are unidentical and the obtained total magnetic moment is 0.698 μ_B. Upon adsorption of NO molecule, the DOS of N 2p and O 2p are highly delocalized and run across the Fermi. There are multiple orbital overlaps of N 2p and O 2p of NO with Ti 3d at −1.5, −0.1, 1.6, 3 eV in spin up and at 0.1, 1.0, 2.0, 3.1 eV in spin down. The overlap area is wider than that of CO_2, CO, H_2S and HF molecules adsorbed systems. This phenomenon shows that the interaction of NO molecule with Ti doped hBN monolayer is the strongest, which supports the large charge transfer and adsorption energy value. The spin up and spin down states are asymmetric and the obtained total magnetic moment of the system is 1.546 μ_B.

From Fig. 5 it can also be noticed that the DOS of all gas molecules mainly hybridize with DOS of Ti atom only. Ti atom acts as charge transferring agent, which enhances the interaction between gas molecules and hBN monolayer. Further, there are only spin up non-zero DOS around the Fermi for all gas molecules adsorbed systems except NO adsorbed system. Thus NO adsorbed system show metallic nature while others show semi metallic.

To understand the charge transfer between gas molecules and Ti doped hBN monolayer quantitatively and visually, we discussed the Bader charge transfer with charge density difference (CDD) diagrams. The charge density difference is calculated by following expression and calculated diagrams are presented in Fig. 6.

$$\Delta\rho = \rho_{\text{gas+Ti-hBN}} - \rho_{\text{Ti-hBN}} - \rho_{\text{gas}} \quad (6)$$

where $\rho_{\text{gas+Ti-hBN}}$ is the charge density of gas molecule adsorbed Ti doped hBN system, $\rho_{\text{Ti-hBN}}$ is the charge density of Ti doped hBN system and ρ_{gas} is the charge density of isolated gas molecule. The yellow region represents the charge gain whereas blue represents the charge loss. For CO_2 adsorption, the charge loss region mainly locates on the Ti atom, while charge gain region is on O atom of CO_2 molecule, illustrating that O atom gains 0.18*e* lost by Ti atom. As to CO molecule, the charge gain

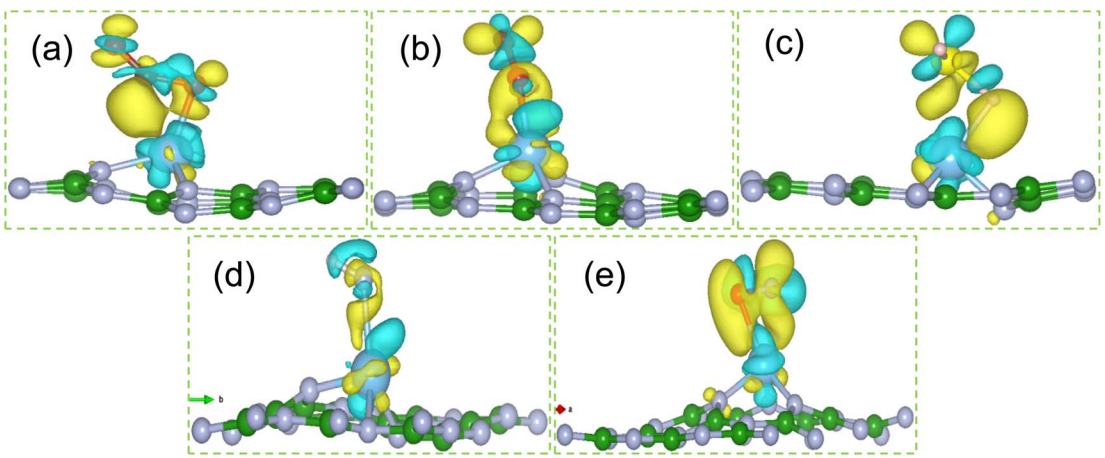

Fig. 6 Charge density difference (CDD) diagrams of (a) CO_2, (b) CO, (c) H_2S, (d) HF and (e) NO molecule adsorbed Ti doped hBN monolayer systems. Cyan and yellow colors represent charge loss and charge gain. Isovalue is taken as 0.003 e $Å^{-1}$.

region is concentrated at O atom of CO molecule whereas the charge loss region is on Ti atom. The 0.21*e* are transferring from Ti atom to O atom of CO molecule. For H_2S, the charge loss region is primarily around H and S atoms. Charge loss region mainly occurs on Ti atom. This means H_2S molecule accepts the 0.16*e* donated by Ti atom. For HF adsorption, the charge gain

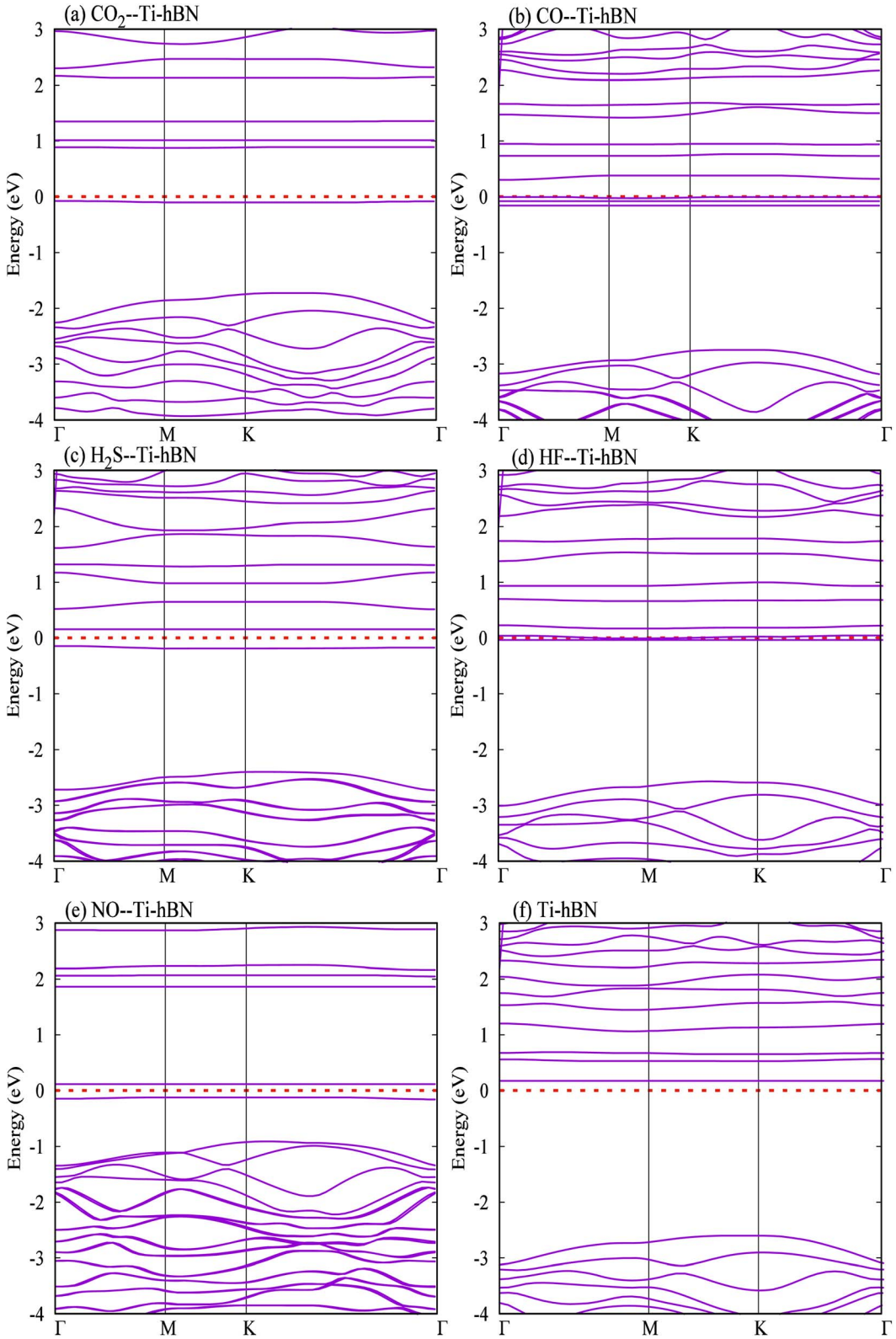

Fig. 7 Electronic band structures of (a) CO_2, (b) CO, (c) H_2S, (d) HF, (e) NO molecule adsorbed Ti doped hBN monolayer systems and (f) Ti doped hBN monolayer. Red dotted horizontal line represents Fermi energy level set at zero.

region is around the F atom. The charge loss is region is mainly on Ti atom, suggesting that HF molecule has gained 0.10*e* charge lost Ti atom. In NO adsorption, there is large charge gain region around the N and O atoms. The charge loss region is primarily on the Ti atom, indicating that NO has gained 0.28*e* charge donated by Ti atom.

From Fig. 6, it can be seen that the charge loss region is Ti atom centered whereas the charge gain region is on the adsorbed gas molecules. This confirmed the quantitative results of Bader charge analysis that adsorbed gas molecules accept the charge from Ti doped hBN monolayer.

3.3.3. Sensitivity and selectivity analysis of Ti doped hBN monolayer. The sensitivity of the semiconducting materials are mostly judged by their electric conductivity (σ), which changes with adsorption of gas molecules, which further can be calculated with following expression.

$$\sigma = AT^{3/2}e^{(-E_g/2K_BT)} \quad (7)$$

where A is a constant, T is the temperature, E_g is the band gap and K_B is Boltzmann's constant, therefore electric conductivity depends on term $e^{(-E_g/2K_BT)}$ at a certain temperature. A change of band gap will cause the change of electric conductivity of the material when it is exposed to gas molecule, manifesting the sensitivity of a gas sensing material. The band structures of CO_2, CO, H_2S, HF, NO adsorbed Ti doped hBN monolayers and Ti doped hBN monolayer (Ti-hBN *i.e.* without gas exposure) are presented in Fig. 7. Compared with Ti-hBN, we found that CO_2 adsorption produces an impurity state in valence band very close to Fermi thereby reducing the band gap from 2.6 to 0.98 eV. CO adsorption induces impurity states at Fermi energy, the impurity states cross to valence band through Fermi and disappear the band gap. In case of H_2S, there appear two impurity states above and below the Fermi at 0.15 and −0.18 eV in conduction and valence band respectively. The appearance of these impurity states narrows down the band gap to 0.33 from 2.6 eV. HF exposure, also produces the impurity states on the Fermi similar to CO, hence there remains no band gap in this case. NO adsorption introduces the impurity states above and below the Fermi similarly to H_2S adsorption, thereby reducing the band gap from 2.6 to 0.11 eV. The calculated values of band gaps (E_g) of CO_2, CO, H_2S, HF and NO gas molecules adsorbed on Ti doped hBN monolayer are listed in Table 2. The band gap variation (ΔE_g) for CO_2, CO, H_2S, HF and NO adsorbed complexes are 62.3, 100, 87.3, 100, 95.7%. Since there is wide difference of band gaps before and after gases exposures, therefore the change in electric conductivity of substrate surely occurs in larger margin.

Further, work function (Φ) is often used to assess the sensitivity of a material when a gas sensor is used as work function type gas sensor, which works based on Kelvin method.[62,63] The Kelvin method is performed by evaluating the Φ of a sensing material before and after gas exposure using Kelvin oscillator tool.[64] The variation of the Φ of sensing material during gas exposure operation would reflect the sensitivity of the sensing material. The calculated values of Φ of Ti doped hBN monolayer with and without gas molecules adsorption are summarized in Table 1. We found that the chemisorptions of CO_2, CO, H_2S, HF and NO on Ti doped hBN monolayer significantly alter the value of Φ (5.31 eV) of Ti doped hBN monolayer to 4.82, 4.70, 4.88, 4.91 and 4.48 eV respectively, whereas the value of Φ for HF adsorption changes to 5.10 eV. The variations of Φ after CO_2, CO, H_2S, HF and NO gas adsorptions are as 9.2, 11.4, 8.0, 7.5 and 15.6%. The variations of Φ in response to CO_2, CO, H_2S, HF and NO gas adsorptions prove that Ti doped hBN monolayer is highly sensitive to all five gases.

The difference in variation of band gaps for CO and HF gases is zero, so Ti doped hBN monolayer is not selective to these gases *i.e.* Ti doped hBN monolayer cannot differentiate the sensing of CO and HF. For H_2S and NO, the variations are 86 and 95% respectively, so selectivity for these two gas molecules is moderate. However the variation of band gap for CO_2 is 62.3%, which indicates that Ti doped hBN monolayer is highly selective to CO_2 gas.

3.4. Application feasibility of Ti doped hBN monolayer as gas sensor

In order to manufacture a practically efficient and high performance gas sensor, the gas adsorption mechanism should be such that the gas can stay on sensor surface to get sensed effectively and be dislodged from the sensor surface without ruining it. In first instant, the gas molecule must remain adsorbed on gas sensing material at room temperature. After successful detection of gas, the gas sensor should recover itself with short recovery time. Secondly, from FPMD simulations of Ti doped hBN monolayer in section 3.3.3 prove that there is no any structural distortion even 1000 K upto 3.5 ps simulation time. So it is therefore assured that Ti doped hBN monolayer is thermodynamically stable.

3.4.1. Analysis of ability of Ti doped hBN monolayer for gas sensing at room temperature. To verify the suitability of Ti doped hBN monolayer in real time application, we have checked its ability of gas sensing at room temperature. Thermodynamic stability of gas sensing material is prerequisite for this purpose. For this, we have carried out the FPMD simulations of gas molecules adsorbed systems at 300 K. Total energies as a function of time of gas adsorbed systems are presented in Fig. 8. After 3.5 ps simulation time, the pictures of resultant structures are displayed as insets in Fig. 8. It is found that no any gas molecule escape from the substrate with increasing simulation time. Ti doped hBN monolayer holds the gas molecules at room temperature. Further, the oscillations of total energy are in the quite small range. This suggests that gas molecules stay adsorbed on Ti doped hBN monolayer at room temperature.

3.4.2. Analysis of recovery time of Ti doped hBN monolayer after gas adsorption. Recovery time of gas sensor is one of the key indicators to evaluate the reusability of a gas sensor. At room temperature (300 K), the values of τ for gas molecules adsorbed on Ti doped hBN monolayer are achieved, 1.46×10^{10}, 7.539×10^{15}, 1.416×10^{8}, 40.03 and 3.641×10^{18} s, for CO_2, CO, H_2S, HF and NO respectively. The recovery time for HF gas is 40 seconds at 300 K with visible light exposure, which is not too

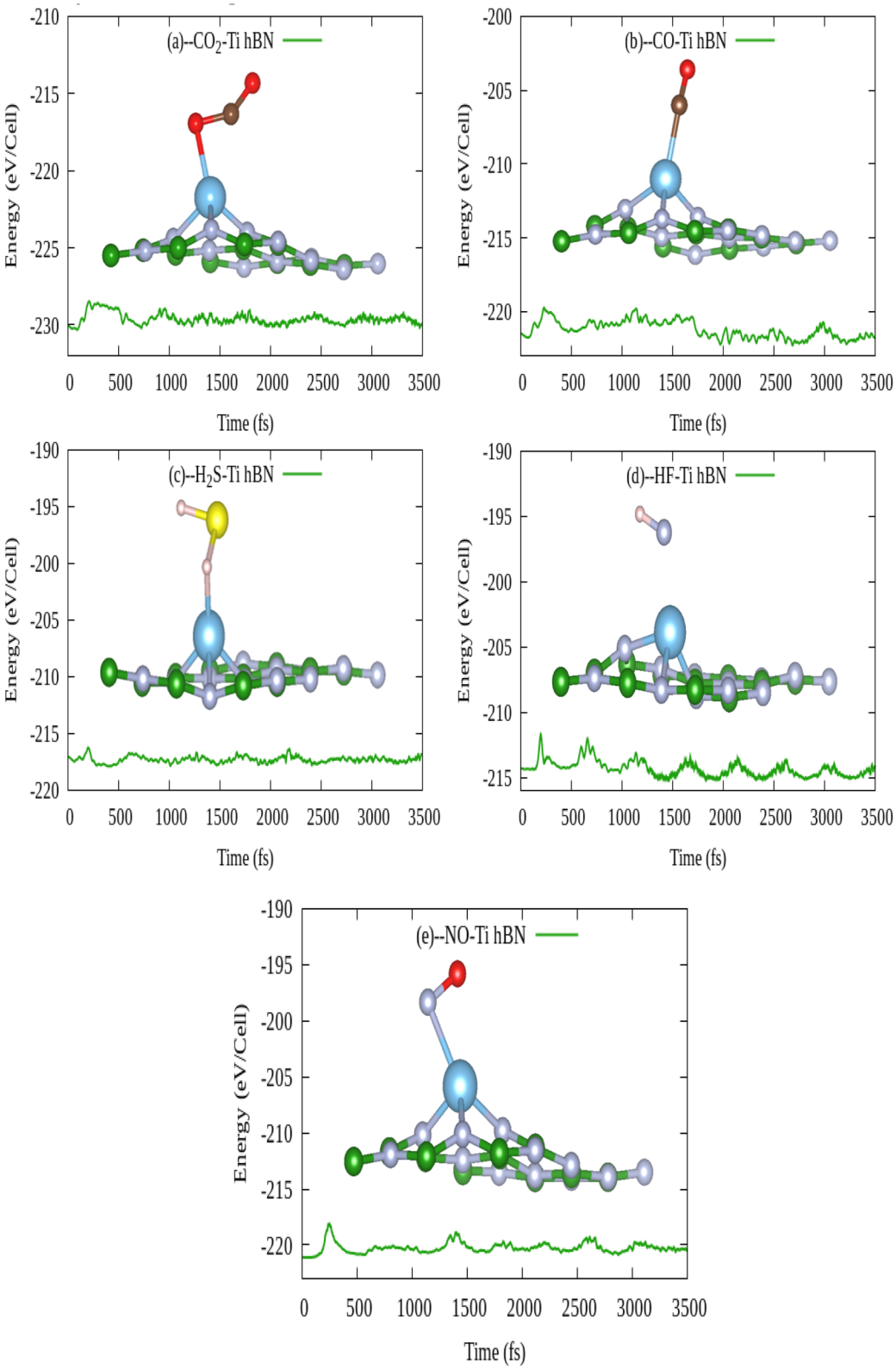

Fig. 8 The fluctuation of total energy of (a) CO_2, (b) CO, (c) H_2S, (d) HF and (e) NO adsorbed Ti doped hBN monolayer systems during FPMD simulations at 300 K. The insets in (a–d) are side views of final structures after 3.5 ps simulation time.

long. Therefore HF gas can easily be desorbed from the surface of Ti doped hBN monolayer and Ti doped hBN monolayer can be repeatedly used for sensing HF gas at room temperature. Whereas, the recovery times required for full desorption of CO_2, CO, H_2S and NO gas molecules from Ti doped hBN monolayer at 300 K are so long. This means that long recovery time precludes

Table 3 Recovery time (τ) in seconds of CO_2, CO, H_2S, HF and NO adsorbed on Ti doped hBN monolayer at 300, 400 and 500 K with visible light and ultra violet exposure

System	τ (s) at 300 K, visible light	τ (s), 400 K, visible light	τ (s), 500 K, visible light	τ (s), 300 K, UV light	τ (s), 400 K, UV light	τ (s), 500 K, UV light
Ti doped hBN-CO_2	1.46×10^{10}	4.214×10^{4}	19.865	1.46×10^{7}	42.147	1.986×10^{-2}
Ti doped hBN-CO	7.539×10^{15}	8.071×10^{8}	5.304×10^{4}	7.53×10^{12}	8.071×10^{5}	53.04
Ti doped hBN-H_2S	1.416×10^{8}	1.298×10^{3}	1.232	1.416×10^{5}	1.298	1.232×10^{-3}
Ti doped hBN-HF	40.039	1.590×10^{-2}	1.446×10^{-4}	4.00×10^{-2}	1.590×10^{-5}	1.446×10^{-7}
Ti doped hBN-NO	3.641×10^{18}	8.357×10^{10}	2.167×10^{6}	3.641×10^{15}	8.357×10^{7}	2.167×10^{3}

the repeatable use of Ti doped hBN monolayer as gas sensor, however the recovery time of gas sensor can be shortened significantly by annealing it at high temperature with ultra violet radiation. Based on expression (2), if adsorption energy E_{ads} is kept constant, either an increasing temperature or attempt frequency (UV light exposure 10^{15} Hz) or both can cause the reduced recovery time. It was also verified that ultra violet radiations assist the quick recovery of the sensor.[65] Therefore, in order to have the quick recovery of Ti doped hBN monolayer, we analyzed the recovery time by annealing at 400 and 500 K in a vacuum (visible light) or UV exposure. The calculated values of recovery time at 300, 400 and 500 K in vacuum and UV exposure are presented in Table 3. By annealing at 400 K in vacuum could not reduce the recovery times of CO_2, CO, H_2S and NO gas molecules significantly, however at 500 K in vacuum CO_2 and H_2S gas molecules can be desorbed within 19.8 and 1.23 seconds respectively. The desorption of CO gas molecules from Ti doped hBN monolayer can be done in reasonable time of 53 seconds by annealing at 500 K with UV exposure. Although the recovery time is significantly shortened by annealing at high temperature and UV exposure, the recovery time is still long enough for NO gas molecule. It takes 6 hours to fully desorb from surface of Ti doped hBN monolayer. Therefore Ti doped hBN monolayer is very suitable as a scavenger for NO gas.

Conclusions

We explored the adsorptions of toxic gas molecules (CO_2, CO, H_2S, HF and NO) on pristine and Ti atom doped hBN monolayer based on first principle calculations. The adsorption of gas molecules on pristine hBN is by physisorption owing to their small adsorption energy and charge transfer. The weak adsorption of gas molecules on pristine hBN results in micro seconds recovery time. Such instantaneous desorption from surface indicates the pristine hBN's poor gas sensing affinity. Ti atom was doped into hBN at N vacancy, B vacancy and BN (Stone Wales) defect. When Ti atom is doped at B vacancy, the doping system is found to be most stable. Further FPMD simulation proved thermodynamic stability of Ti doped hBN monolayer up to 1000 K. After Ti atom doping, the adsorption energy of gas molecules increases considerably, resulting in chemisorption. The outermost orbitals of Ti atom, atoms of gas molecules and boron and nitrogen show strong hybridization in PDOS plots confirming the strong interaction of gas molecules with Ti doped hBN monolayer. Bader charge analysis reveals that Ti atom donates charge to gas molecules. The electronic properties of Ti doped hBN monolayer greatly change after gas molecules adsorption. The band gap of Ti doped hBN monolayer narrows to 0.91, 0.36 and 0.13 from 2.61 eV with CO_2, H_2S and NO adsorptions respectively while it changes to zero gap (metallic) with CO and HF adsorption. Such large change in band gap and work function indicates that Ti doped hBN monolayer is highly sensitive to these gases. However, due to same variation of work function in response to HF and NO gas adsorptions, Ti doped hBN monolayer is said to not selective to adsorptions of these two gases. Furthermore, reusability of sensor is evaluated by recovery time of gas molecules desorption. The gas molecules except NO can be desorbed by increasing temperature to 500 K with UV radiation within reasonable recovery time. The desorption of NO molecule takes 6 hours even at 500 K with UV exposure, that is why Ti doped hBN monolayer is better to be a scavenger of this gas rather than gas sensor. Overall, Ti doped hBN monolayer is predicted to be promising material for gas sensor of CO_2, CO, H_2S and HF and scavenger for NO gas.

Conflicts of interest

The authors declare that they have no known competing financial interests or personal relationships that could have appeared to influence the work reported in this paper.

References

1 J. Lelieveld, J. S. Evans, M. Fnais, D. Giannadaki and A. Pozzer, The contribution of outdoor air pollution sources to premature mortality on a global scale, *Nature*, 2015, **525**, 367–371.
2 Z. Li, N. Wang, Z. Lin, J. Wang, W. Liu, K. Sun, *et al.*, Room-temperature high-performance H_2S sensor based on porous CuO nanosheets prepared by hydrothermal method, *ACS Appl. Mater. Interfaces*, 2016, **8**, 20962–20968.
3 J. Lindenmann, V. Matzi, N. Neuboeck, B. Ratzenhofer-Komenda, A. Maier and F.-M. Smolle-Juettner, Severe hydrogen sulphide poisoning treated with 4-dimethylaminophenol and hyperbaric oxygen, *Diving Hyperb Med*, 2010, **40**, 213–217.
4 A. L. Chiew and N. A. Buckley, Carbon monoxide poisoning in the 21st century, *J. Crit. Care*, 2014, **18**, 1–8.

5 L. H. Ziska and K. L. Ebi, Climate change, carbon dioxide, and public health: the plant biology perspective, in *Global Climate Change and Human Health: From Science to Practice*, 2021, p. 131.
6 H. Shin, S. K. Oh, H. Y. Lee, H. Chung, S. Y. Yoon and S. Y. Choi, Comparative Analysis of Hydrogen Fluoride-Exposed Patients Based on Major Burn Criteria After the 2012 Gumi City Chemical Leak Disaster, *J. Burn Care Res.*, 2021, 834–840.
7 A. A. Khan, M. D. Esrafili, F. Ali, R. Ahmad and I. Ahmad, Silicon-doped boron nitride graphyne-like sheet for catalytic N_2O reduction: a DFT study, *J. Mol. Graphics Modell.*, 2022, 108186.
8 X. Tang, A. Du and L. Kou, Gas sensing and capturing based on two-dimensional layered materials: overview from theoretical perspective, *Wiley Interdiscip. Rev.: Comput. Mol. Sci.*, 2018, **8**, e1361.
9 M. Donarelli and L. Ottaviano, 2D materials for gas sensing applications: a review on graphene oxide, MoS2, WS2 and phosphorene, *Sensors*, 2018, **18**, 3638.
10 I. Gablech, J. Pekárek, J. Klempa, V. Svatoš, A. Sajedi-Moghaddam, P. Neužil, *et al.*, Monoelemental 2D materials-based field effect transistors for sensing and biosensing: phosphorene, antimonene, arsenene, silicene, and germanene go beyond graphene, *TrAC, Trends Anal. Chem.*, 2018, **105**, 251–262.
11 C. Feng, H. Qin, D. Yang and G. Zhang, First-principles investigation of the adsorption behaviors of CH_2O on BN, AlN, GaN, InN, BP, and P monolayers, *Materials*, 2019, **12**, 676.
12 N. Joshi, M. L. Braunger, F. M. Shimizu, A. Riul and O. N. Oliveira, Two-dimensional transition metal dichalcogenides for gas sensing applications, *Nanosensors for Environmental Applications*, Springer, 2020, pp. 131–155.
13 P. Goswami and G. Gupta, Recent progress of flexible NO_2 and NH_3 gas sensors based on transition metal dichalcogenides for room temperature sensing, *Mater. Today Chem.*, 2022, **23**, 100726.
14 M. V. Nikolic, V. Milovanovic, Z. Z. Vasiljevic and Z. Stamenkovic, Semiconductor gas sensors: materials, technology, design, and application, *Sensors*, 2020, **20**, 6694.
15 C. Anichini, W. Czepa, D. Pakulski, A. Aliprandi, A. Ciesielski and P. Samorì, Chemical sensing with 2D materials, *Chem. Soc. Rev.*, 2018, **47**, 4860–4908.
16 Y. Zeng, S. Lin, D. Gu and X. Li, Two-dimensional nanomaterials for gas sensing applications: the role of theoretical calculations, *Nanomaterials*, 2018, **8**, 851.
17 S.-Y. Xia, L.-Q. Tao, T. Jiang, H. Sun and J. Li, Rh-doped h-BN monolayer as a high sensitivity SF6 decomposed gases sensor: a DFT study, *Appl. Surf. Sci.*, 2021, **536**, 147965.
18 L. Palomino-Asencio, E. Chigo-Anota and E. García-Hernández, Insights on α-Glucose Biosensors/Carriers Based on Boron-Nitride Nanomaterials from an Atomistic and Electronic Point of View, *ChemPhysChem*, 2022, e202200310.
19 J. Ren, L. Stagi and P. Innocenzi, Hydroxylated boron nitride materials: from structures to functional applications, *J. Mater. Sci.*, 2021, **56**, 4053–4079.
20 W. Luo, Y. Wang, E. Hitz, Y. Lin, B. Yang and L. Hu, Solution processed boron nitride nanosheets: synthesis, assemblies and emerging applications, *Adv. Funct. Mater.*, 2017, **27**, 1701450.
21 H. Wang, L. Tian, Z. Huang, F. Liang, K. Guan, Q. Jia, *et al.*, Molten salt synthesis of carbon-doped boron nitride nanosheets with enhanced adsorption performance, *Nanotechnology*, 2020, **31**, 505606.
22 N. Briggs, S. Subramanian, Z. Lin, X. Li, X. Zhang, K. Zhang, *et al.*, A roadmap for electronic grade 2D materials, *2D Materials*, 2019, **6**, 022001.
23 B. J. Matsoso, C. Garcia-Martinez, T. H. Mongwe, B. Toury, J. P. Serbena and C. Journet, Room temperature ammonia vapour detection on hBN flakes, *J. Phys.: Mater.*, 2021, **4**, 044007.
24 M. Legesse, S. N. Rashkeev, H. Saidaoui, F. El Mellouhi, S. Ahzi and F. H. Alharbi, Band gap tuning in aluminum doped two-dimensional hexagonal boron nitride, *Mater. Chem. Phys.*, 2020, **250**, 123176.
25 K. Zhang and J. Robinson, Doping of two-dimensional semiconductors: a rapid review and outlook, *MRS Adv.*, 2019, **4**, 2743–2757.
26 K. Fatima, M. Rafique, A. M. Soomro and M. Kumar, Activation of h-BN and SiC monolayer sheets through foreign atom substitution; a comparative study based on *ab initio* method, *J. Chin. Chem. Soc.*, 2022, 1585–1593.
27 K. Singh, M. Kaur, I. Chauhan, A. Awasthi, M. Kumar, A. Thakur, *et al.*, BN/NiO nanocomposites: structural, defect chemistry and electrical properties in hydrogen gas atmosphere, *Ceram. Int.*, 2020, **46**, 26233–26237.
28 K. Zhang, Y. Feng, F. Wang, Z. Yang and J. Wang, Two dimensional hexagonal boron nitride (2D-hBN): synthesis, properties and applications, *J. Mater. Chem. C*, 2017, **5**, 11992–12022.
29 S. R. Naqvi, V. Shukla, N. K. Jena, W. Luo and R. Ahuja, Exploring two-dimensional M_2NS_2 (M = Ti, V) MXenes based gas sensors for air pollutants, *Appl. Mater. Today*, 2020, **19**, 100574.
30 Y. C. Lin, R. Torsi, D. B. Geohegan, J. A. Robinson and K. Xiao, Controllable Thin-Film Approaches for Doping and Alloying Transition Metal Dichalcogenides Monolayers, *Adv. Sci.*, 2021, **8**, 2004249.
31 J. Ramirez-de-Arellano and L. Magana-Solis, Interaction of CO with an hBN surface doped with Ti and Pt: a first principles study, *J. Phys.: Conf. Ser.*, 2017, 012074.
32 Y. Wang, Y. Du, Y. Meng, B. Xie, Z. Ni and S. Xia, Monatomic Ti doped on defective monolayer boron nitride as an electrocatalyst for the synthesis of ammonia: a DFT study, *Appl. Surf. Sci.*, 2021, **563**, 150277.
33 S.-Y. Zhong, S.-Y. Wu, X.-Y. Yu, G.-Q. Shen, L. Yan and K.-L. Xu, First-Principles Studies of the Adsorption and Catalytic Properties for Gas Molecules on h-BN Monolayer Doped with Various Transition Metal Atoms, *Catal. Surv. Asia*, 2021, 1–11.
34 E. C. Anota, 2D boron nitride incorporating homonuclear boron bonds: stabilized in neutral, anionic and cationic charge, *SN Appl. Sci.*, 2022, **4**, 1–8.

35 B. Liu and K. Zhou, Recent progress on graphene-analogous 2D nanomaterials: properties, modeling and applications, *Prog. Mater. Sci.*, 2019, **100**, 99–169.
36 A. B. Hernández, E. C. Anota, F. S. Carrillo, O. V. Cuchillo and M. S. Villanueva, *In silico* study of the adsorption of H_2, CO and CO_2 chemical species on $(TiO_2)_n$ n = 15–20 clusters: the (TiO_2) 19 case as candidate promising, *J. Mol. Graphics Modell.*, 2022, **117**, 108316.
37 B. A. Kalwar, W. Fangzong, M. H. Saeed, A. A. Bhutto, M. A. Tunio and K. Bhagat, Geometric, spintronic, and opto-electronic properties of 3d transition metals doped silicene: an *ab initio* study, *J. Chin. Chem. Soc*, 2022, 1706–1718.
38 B. A. Kalwar, W. Fangzong, I. Ahmed and M. H. Saeed, Ti atom doped single vacancy silicene for hydrogen energy storage: DFT study, *J. Chin. Chem. Soc.*, 2021, **68**, 2243–2253.
39 E. Chigo Anota, A. Escobedo-Morales, M. Salazar Villanueva, O. Vázquez-Cuchillo and E. Rubio Rosas, On the influence of point defects on the structural and electronic properties of graphene-like sheets: a molecular simulation study, *J. Mol. Model.*, 2013, **19**, 839–846.
40 W. Tang, E. Sanville and G. Henkelman, A grid-based Bader analysis algorithm without lattice bias, *J. Phys.: Condens. Matter*, 2009, **21**, 084204.
41 J. Hafner, *Ab initio* simulations of materials using VASP: density-functional theory and beyond, *J. Comput. Chem.*, 2008, **29**, 2044–2078.
42 J. P. Perdew, K. Burke and M. Ernzerhof, Generalized gradient approximation made simple, *Phys. Rev. Lett.*, 1996, **77**, 3865.
43 P. E. Blöchl, Projector augmented-wave method, *Phys. Rev. B: Condens. Matter Mater. Phys.*, 1994, **50**, 17953.
44 H. J. Monkhorst and J. D. Pack, Special points for Brillouin-zone integrations, *Phys. Rev. B: Condens. Matter Mater. Phys.*, 1976, **13**, 5188.
45 S. Grimme, Semiempirical GGA-type density functional constructed with a long-range dispersion correction, *J. Comput. Chem.*, 2006, **27**, 1787–1799.
46 R. F. Bader and P. Beddall, Virial field relationship for molecular charge distributions and the spatial partitioning of molecular properties, *J. Chem. Phys.*, 1972, **56**, 3320–3329.
47 K. Momma and F. Izumi, VESTA 3 for three-dimensional visualization of crystal, volumetric and morphology data, *J. Appl. Crystallogr.*, 2011, **44**, 1272–1276.
48 R. Muhammad, M. A. Uqaili, Y. Shuai, M. A. Mahar and I. Ahmed, *Ab initio* investigations on the physical properties of 3d and 5d transition metal atom substituted divacancy monolayer h-BN, *Appl. Surf. Sci.*, 2018, **458**, 145–156.
49 R. Peng, Q. Zhou and W. Zeng, First-Principles Study of Au-Doped InN Monolayer as Adsorbent and Gas Sensing Material for SF6 Decomposed Species, *Nanomaterials*, 2021, **11**, 1708.
50 X. Gao, Q. Zhou, J. Wang, L. Xu and W. Zeng, Performance of Intrinsic and Modified Graphene for the Adsorption of H_2S and CH_4: A DFT Study, *Nanomaterials*, 2020, **10**, 299.
51 A. Aasi, S. Mehdi Aghaei and B. Panchapakesan, Outstanding performance of transition-metal-decorated single-layer graphene-like BC6N nanosheets for disease biomarker detection in human breath, *ACS Omega*, 2021, **6**, 4696–4707.
52 P. Hänggi, P. Talkner and M. Borkovec, Reaction-rate theory: fifty years after Kramers, *Rev. Mod. Phys.*, 1990, **62**, 251.
53 M. Miletic, K. Palczynski and J. Dzubiella, Quantifying entropic barriers in single-molecule surface diffusion, *J. Chem. Phys.*, 2020, **153**, 164713.
54 H. L. Chia, C. C. Mayorga-Martinez and M. Pumera, Doping and decorating 2D materials for biosensing: benefits and drawbacks, *Adv. Funct. Mater.*, 2021, **31**, 2102555.
55 M. Rafique, M. A. Uqaili, N. H. Mirjat, M. A. Tunio and Y. Shuai, *Ab initio* investigations on titanium (Ti) atom-doped divacancy monolayer h-BN system for hydrogen storage systems, *Phys. E*, 2019, **109**, 169–178.
56 J. Zhao and Z. Chen, Single Mo atom supported on defective boron nitride monolayer as an efficient electrocatalyst for nitrogen fixation: a computational study, *J. Am. Chem. Soc.*, 2017, **139**, 12480–12487.
57 M. Wang, F. Meng, D. Hou, Y. Han, J. Ren, C. Bai, *et al.*, Electronic structure and spin properties study on 2D h-BN nanosheet with Ti or Fe doping, *Solid State Commun.*, 2020, **307**, 113803.
58 D.-H. Kim, H.-S. Kim, M. W. Song, S. Lee and S. Y. Lee, Geometric and electronic structures of monolayer hexagonal boron nitride with multi-vacancy, *Nano Convergence*, 2017, **4**, 1–8.
59 N. Promthong, C. Tabtimsai, W. Rakrai and B. Wanno, Transition metal-doped graphene nanoflakes for CO and CO_2 storage and sensing applications: a DFT study, *Struct. Chem.*, 2020, **31**, 2237–2247.
60 H. N. Vergara-Reyes, M. Acosta-Alejandro and E. Chigo-Anota, Quantum-mechanical assessment of the adsorption of nitric oxide molecules on the magnetic carbon nitride $(C_{36}N_{24})^-$ fullerene, *Struct. Chem.*, 2021, **32**, 1775–1786.
61 E. Clementi and D.-L. Raimondi, Atomic screening constants from SCF functions, *J. Chem. Phys.*, 1963, **38**, 2686–2689.
62 D. Chen, Y. Li, S. Xiao, C. Yang, J. Zhou and B. Xiao, Single Ni atom doped WS2 monolayer as sensing substrate for dissolved gases in transformer oil: a first-principles study, *Appl. Surf. Sci.*, 2022, **579**, 152141.
63 Y. Yong, R. Gao, X. Wang, X. Yuan, S. Hu, Z. Zhao, *et al.*, Highly sensitive and selective room-temperature gas sensors based on $B_6N_6H_6$ monolayer for sensing SO_2 and NH_3: a first-principles study, *Results Phys.*, 2022, **33**, 105208.
64 D. Chidambaram, R. Kalidoss, K. Pushparaj, V. J. Surya and Y. Sivalingam, Post-deposition annealing influences of gas adsorption on semi-vertical β-FeOOH nanorods at room temperature: a scanning kelvin probe analysis, *Mater. Sci. Eng., B*, 2022, **280**, 115694.
65 T. Li, D. Zhang, Q. Pan, M. Tang and S. Yu, UV enhanced NO_2 gas sensing at room temperature based on coral-like tin diselenide/MOFs-derived nanoflower-like tin dioxide heteronanostructures, *Sens. Actuators, B*, 2022, **355**, 131049.